Self-sealing Microarc Oxidation Coating Mainly Containing ZrO_2 and Nano $Mg_2Zr_5O_{12}$ on AZ91D Mg Alloy

Mingqi Tang[1,*], Yufei Shao[2], Zaiqiang Feng[1], Wen Wang[2], Gang Li[1], Zhenwei Yan[2], and Ruizhu Zhang[1]

[1] School of Materials Science and Engineering, North China University of Water Resources and Electric Power, Zhengzhou 450045, China
[2] School of Mechanical Engineering, North China University of Water Resources and Electric Power, Zhengzhou 450045, China
[*]E-mail: tangmq400@163.com

ZrO_2-Mg_2ZrO_{12}-MgO composite oxide coating was obtained on AZ91D Mg alloy via MAO (microarc oxidation) technique in an alkaline phosphate solution with K_2ZrF_6 and ZrO_2 nanoparticles. The influence of K_2ZrF_6 and ZrO_2 nanoparticles on the thickness, microstructure, elemental composition, and anti-corrosion property of the MAO coatings were investigated. Added K_2ZrF_6 in the solution improved the forming efficiency of MAO coating. Due to the self-sealing effect of $ZrO_2 \cdot nH_2O$ colloid particles produced by K_2ZrF_6 hydrolysis, the hole size and quantity in the MAO coating surface decreased. Moreover, K_2ZrF_6 induced nano-Mg_2ZrO_{12} to appear in the MAO coating. On the contrary, the MAO coating prepared in the K_2ZrF_6 free solution composed mainly of MgO and non-crystal phosphate. The MAO coating had better compactness and anti-corrosion property which fabricated in the solution with 10 g/L K_2ZrF_6. The thickness, compactness, and anti-corrosion property of the MAO coating were further enhanced because of the addition of ZrO_2 nanoparticles in the solution containing 10 g/L K_2ZrF_6.

Keywords: Mg alloy; Microarc oxidation; Zirconia; Self-sealing；Anti-corrosion property

1. INTRODUCTION

Microarc oxidation (MAO) technique can produce ceramic oxide coatings solidly bonded to Mg and its alloys, remarkably improve their anti-corrosion property [1-3]. The phase components of MAO coatings on Mg alloys are MgO and other minerals originated from solutions, such as $MgSiO_4$, $Mg_3(PO_4)_2$, $MgAl_2O_4$, Mg_2ZrO_5, Mg_2TiO_4, TiO_2, ZrO_2, and MgF_2 [4, 5]. In moist or acidic environments, MgO would absorb water to swell and dissolve, and the coating cannot effectively protect Mg alloy substrates in the long term [6-8]. Therefore, MAO coating on Mg alloy with excellent chemical stability

and compact structure should be prepared through harnessing the characteristics of MAO solution to participate in coating formation.

ZrO_2 has such characteristics as high hardness, low thermal conductivity, good thermal and chemical stability. It has been widely used in the preparation of anti-resistant coating, anti-corrosion coating, thermal barrier coatings, and other surface protection coatings [9,10]. ZrO_2 can be introduced into MAO coating to improve its chemical stability and protective effect. In previous studies, researchers added a small amount of sodium acetate, oxalic acid, phosphoric acid, phosphate, and other additives to K_2ZrF_6 solution to prepare MAO coating consisting primarily of ZrO_2, $Mg_2Zr_5O_{12}$, MgF_2, and a small amount of MgO [8, 11-20]. These coatings exhibited better density, chemical durability, and anti-corrosion property than the coatings composed mainly of MgO. However, these solutions are acidic and corrosive to Mg alloy substrates and MAO equipment.

In order to avoid dissolution of Mg alloys in acidic K_2ZrF_6 solution, Lee [21,22] used an alkaline phosphate and an acidic K_2ZrF_6 solution to obtain oxide coatings via a two-step MAO technique. The final MAO coating consisted mostly of $Mg_2Zr_5O_{12}$, ZrO_2, and a small amount of MgO and MgF_2. The anti-corrosion property of MAO coating was drastically improved because of fewer micropores. Z.U. Rehman's research showed that the MAO coatings obtained via the two-step method showed better compactness and chemical stability, and their hardness and anti-corrosion property were markedly improved [23]. However, two-step MAO increased the processing steps, that was a limitation.

The previous researches showed that MAO coatings consisting mainly of ZrO_2, $Mg_2Zr_5O_{12}$ and MgF_2 can also be prepared using alkaline K_2ZrF_6 solutions [24-32]. Cai [26] prepared MAO coatings composed of Al_2O_3, ZrO_2, MgO, MgF_2, and $MgAl_2O_4$ in a solution consisting of $NaAlO_2$, K_2ZrF_6, and KOH on AZ91D Mg alloy. Research by Cui showed that self-sealing MAO coatings consisting of t-ZrO_2, $MgSiO_3$, MgF_2, MgO, and non-crystal phosphate were prepared in K_2ZrF_6-containing solution [27]. These coatings were denser, less defective, and exhibited better anti-corrosion property. Mu obtained three types of MAO coatings using three different solutions of K_2ZrF_6, $NaAlO_2$, and Na_2SiO_3, respectively [30]. The MAO coating prepared in K_2ZrF_6 solution mainly consisted of t-ZrO_2, $Mg_2Zr_5O_{12}$, and MgF_2, which was the densest and showed the best anti-corrosion property. In a solution consisting of K_2ZrF_6, $NH_4H_2PO_4$, and $C_6H_{12}N_4$, Liu prepared oxide coatings composed of ZrO_2, MgF_2, and MgO on Mg alloys by MAO. ZrO_2 was homogeneously distributed in the whole coatings, MgF_2 was largely existed in the holes and cracks of the coatings, and MgO was predominantly present in the internal dense layer near the substrate [33, 34].

MAO coatings with better anti-corrosion properties can be obtained in alkaline solutions containing K_2ZrF_6, but those solutions are generally unstable. With time extension, $ZrO_2 \cdot nH_2O$ particles produced by ZrF_6^{2-} hydrolysis will reunite and convert to $ZrO_2 \cdot nH_2O$ precipitation, which is difficult to disperse, resulting in reduced performance of the MAO coatings or no coatings can be prepared in those solutions. Many investigations have indicated that ZrO_2 particles in the MAO solution of Mg alloys can continuously enter the oxide coatings under the driving action of electric force and mechanical stirring, reduce the size and quantity of holes in the MAO coating [2,4,35-43]. These particles undergo reactions of crystal transformation under the high temperature of discharge spark and react with MgO to produce Mg_2ZrO_5, and reduce the MgO content in the oxide coatings. As a result, the compactness, chemical durability, and anti-corrosion property of the MAO coating have been enhanced. However, most MAO

solutions for magnesium alloy will be difficult to prepare a complete MAO coating or cannot form a coating at all after being stopped for a short period of one or two days [44].

In previous works, K_2TiF_6 and K_2ZrF_6 was added to solutions consisting of $(NaPO_3)_6$, NaOH, and $(HOCH_2CH_2)_3N$ to produce TiO_2 and ZrO_2 colloidal particles via in situ hydrolysis through synergy between those components [45-48]. During MAO process, TiO_2 colloidal particles participated in coating formation and improved the thickness, compactness, and anti-corrosion property of the MAO coating on Mg alloys. Moreover, these solutions were stable and could still be normally used for more than one year. In this study, K_2ZrF_6 and ZrO_2 nanoparticles were added in a base solution consisting of $(NaPO_3)_6$, NaOH, and $(HOCH_2CH_2)_3N$ to fabricate MAO coating on AZ91D Mg alloy. The aims were to develop a novel and stable MAO solution with K_2ZrF_6, obtain oxide coating containing zirconium oxides, and increase the anti-corrosion property of Mg alloy.

2. EXPERIMENTAL

Specimens of AZ91D Mg alloy with $\Phi25 \times 8$ were used as the substrates. A base solution containing $(NaPO_3)_6$ (6 g/L), NaOH (3 g/L), and $(HOCH_2CH_2)_3N$ (10 ml/L) was modified with various content K_2ZrF_6 from 0 to 16 g/L. In addition, t-ZrO_2 nanoparticles (Nanjing Mingshan advanced materials, China) of about 200 nm was used as an additive of the solution with optimum K_2ZrF_6 content. After added ZrO_2 nanoparticles, the solution was treated by ultrasonically dispersing for 30 min and then mechanical stirring for 30 min prior to MAO, and the mechanical agitation was maintained throughout the whole MAO process.

The MAO treatment of AZ91D Mg alloy was performed by using a pulsed electrical source (JX-MAO, Lanzhou Jingxin, China) providing positive pulse voltages. During the MAO process, AZ91D sample was anode, and a sheet of stainless steel (dimension: $60 \times 40 \times 1$ mm) was used as cathode. The MAO parameters are described in Reference [49].

The thickness of the MAO coatings was assessed by an eddy thickness gauge (Time2284, China). The morphologies of the coatings were assessed by a scanning electron microscopy (SEM, FEI, Quanta 2000, Japan), while its chemical composition was determined by an energy dispersion X-ray spectrometry (EDS, OXFORD LINK ISIS, UK). The phases of the coatings were identified by a X–ray diffraction (XRD, Bruker D8 ADVANCE) with a scanning speed of 6 °/min. The microstructure of the coatings was also investigated by a transmission electron microscopy (TEM, JEM-2100F, Japan). The method of preparation TEM sample was elaborated in Reference [47].

The anti-corrosion property of the coatings was examined by electrochemical impedance spectroscopy (EIS) test via an electrochemical workstation (CHI-660E) and a three-electrode cell. At least 5 samples were tested at each condition for adequate statistics. The experiment parameters and details were used as described in previous studies [48,49].

3. RESULTS AND DISCUSSION

3.1 Effect of K_2ZrF_6

Fig. 1 indicates the average thicknesses of the MAO coatings prepared in the solution with various content of K_2ZrF_6. With the increasing of K_2ZrF_6 content, the thicknesses of the coating increased firstly and then decreased. The coating formed in the K_2ZrF_6 free solution was about 22 μm, which fabricated in the solution with 10 g/L K_2ZrF_6 increased to about 35 μm. However, the coating thickness gradually decreased when K_2ZrF_6 content exceeded 10 g/L. K_2ZrF_6 was hydrolyzed to produce $ZrO_2 \cdot nH_2O$ colloidal particles, K^+ and F^- in alkaline solutions. On one hand, $ZrO_2 \cdot nH_2O$ colloidal particles originated from K_2ZrF_6 increased the coating formation rate, and on the other hand, F^- decreased the coating formation rate. As a result, the coating thickness was the highest in the solution with 10 g/L K_2ZrF_6.
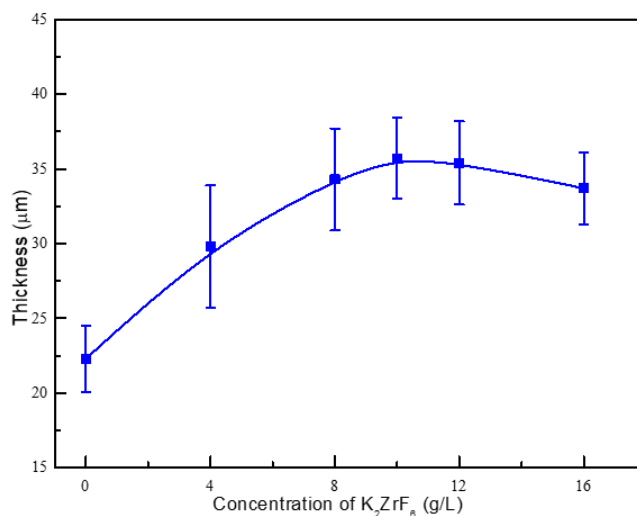

Figure 1. The average thickness of the MAO coatings prepared in the base solution with various content of K_2ZrF_6.

Fig. 2 provides the surface morphology of the MAO coatings prepared in the solution with various content of K_2ZrF_6. Numerous holes and granular attachments of varying sizes appear on the surface of the coatings. These holes and attachments were caused by spark discharge. It can be seen that K_2ZrF_6 addition drastically changed the surface micromorphology of the coatings. For the coating formed in the K_2ZrF_6 free solution, the diameter of the hole was reached about 40 μm. K_2ZrF_6 content was within 0–10 g/L, and as more amounts of K_2ZrF_6 were added, the diameter of the discharge holes gradually decreased. For the coating formed in the solution with K_2ZrF_6, the hole size was less than 10 μm. When the K_2ZrF_6 content exceeded 10 g/L, the size of the discharge hole gradually increased. In addition, numerous holes in MAO coatings prepared in the solutions with K_2ZrF_6 were filled with sediments, rendering them closed or semiclosed. Thus, the addition of K_2ZrF_6 provided the solution with self-sealing effect. In the solution with K_2ZrF_6 content of 10 g/L, most holes on the coating surface were

enclosed by sediments, and only few micropores with smaller apertures were not closed, as shown in Fig. 2(d). K_2ZrF_6 was hydrolyzed in an alkaline solution to produce $ZrO_2 \cdot nH_2O$ colloidal particles that absorb negative charges from the surface [27, 47]. In MAO process, adsorption of negatively charged $ZrO_2 \cdot nH_2O$ colloidal particles that absorb negative charge could enter the channel produced by the spark discharges under the effects of electric field and mechanical agitation. These particles participated in a series of MAO reactions with the components from substrate and solution in the discharge channels. The reaction products were then deposited in the discharge channel due to rapid cooling of the surrounding solution, thereby closing the remaining holes. With increasing of K_2ZrF_6 content in the solution, the number of $ZrO_2 \cdot nH_2O$ particles increased, and its role in filling closed holes became extensive. Therefore, the size and quantity of holes in the MAO coating both decreased. As provided in Fig. 2(e) and Fig. 2(f), the size and quantity of holes in the coatings increased when K_2ZrF_6 content exceeded 10 g/L. The $ZrO_2 \cdot nH_2O$ colloidal particles increased in size with further increasing of the K_2ZrF_6 content due to agglomeration of small $ZrO_2 \cdot nH_2O$ particles. Meanwhile, the electric field force and mechanical agitation on the particles' driving effect would be weakened. It possibly became difficult for $ZrO_2 \cdot nH_2O$ particles to enter the discharge channel, and the self-sealing effect would reduce. This result suggested that the $ZrO_2 \cdot nH_2O$ colloidal particles play the decisive role in the solution's self-sealing effect. The holes were weak positions in the MAO coatings and even accelerated the corrosion rate of the substrate as a transmission channel for Cl^- ions [3, 50]. The solution containing K_2ZrF_6 showed self-sealing effect, the MAO coating could effectively isolate the substrate from external moist environment, thereby enhanced the anti-corrosion property of Mg alloys.

The chemical composition of the MAO coating fabricated in the solution with various content of K_2ZrF_6 are compiled in Table 1. The coating obtained in the solution without K_2ZrF_6 was consisted primarily of O, P, Na, Mg, and Al. Added K_2ZrF_6 caused the appearance of K, Zr, and F in the MAO coatings, and their contents increased with the increasing of K_2ZrF_6 content. Moreover, K_2ZrF_6 reduced the contents of O, Mg, P, Al, and other elements on the coatings surface. The decrease in the content of Mg elements indicated that the contents of the associated MgO and $Mg_3(PO_4)_2$ were reduced, and this reduction was helpful to increase the chemical durability and anti-corrosion property of the MAO coating.

Table 1. Chemical composition of the MAO coatings prepared in the base solution with various content of K_2ZrF_6.

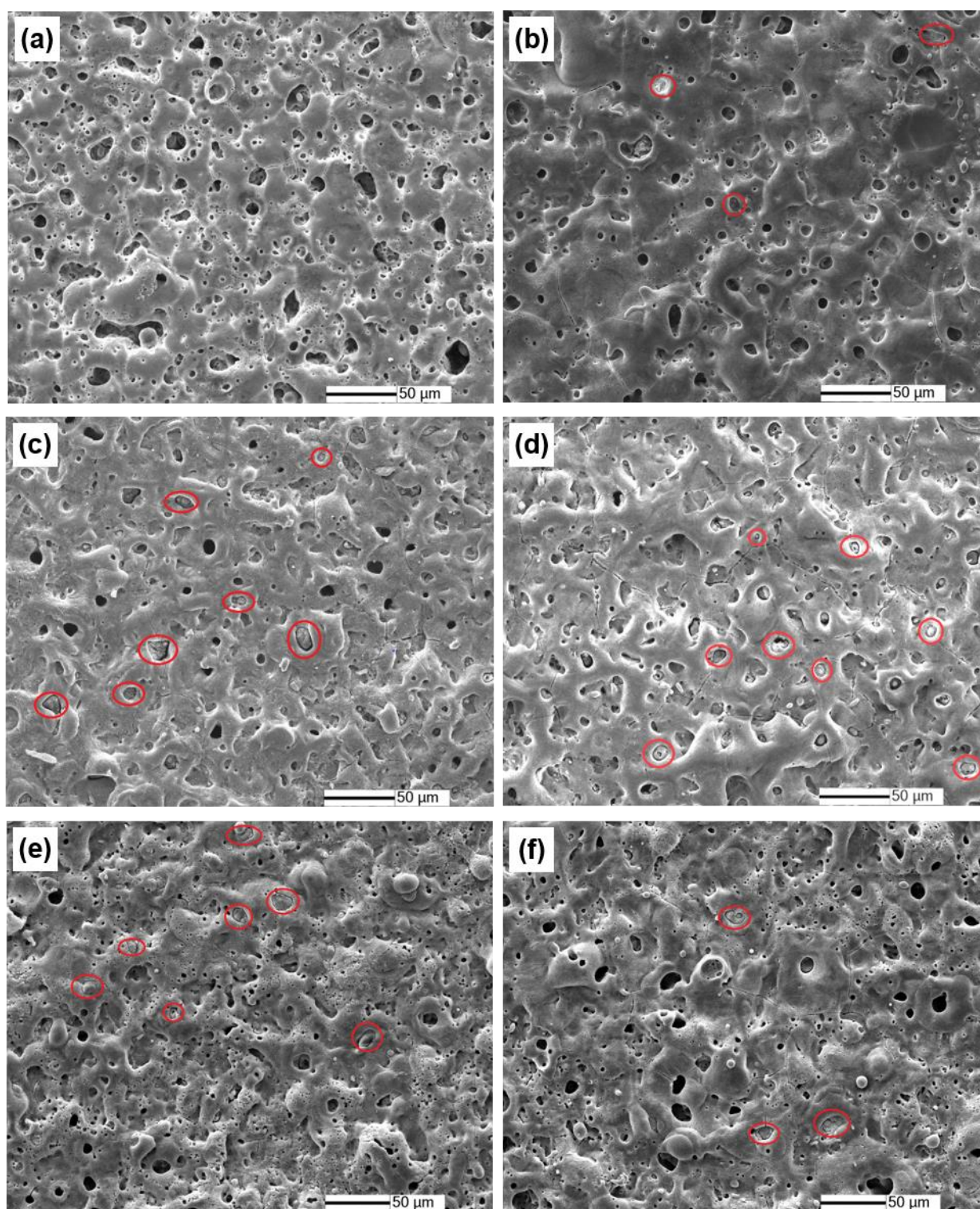| Content of K_2ZrF_6	Element composition (at.%)							
(g/L)	O	P	Mg	Al	Na	Zr	F	K
0	50.3	13.1	32.9	2.0	1.7		-	-
4	51.9	8.7	30.2	0.7	2.0	4.3	2.4	0.4
8	50.5	7.1	28.1	0.4	2.3	5.6	5.7	0.4
10	48.4	6.6	28.8	0.5	1.7	6.9	6.4	0.5
12	47.2	5.4	29.6	0.5	1.9	8.1	6.7	0.7
16	47.9	4.8	27.6	0.6	2.0	9.2	6.9	1.0

Figure 2. Surface micromorphology of the MAO coatings prepared in the base solution with various content of K_2ZrF_6, (a) 0 g/L, (b) 4 g/L, (c) 8 g/L, (d) 10 g/L, (e) 12 g/L, and (f) 16 g/L.

XRD patterns of the MAO coating prepared in the solution with various content of K_2ZrF_6 are displayed in Fig. 3. For the coating prepared in the K_2ZrF_6 free solution, the peak of MgO and Mg were defined, as shown in Fig. 3(a). Phosphorus element was detected by EDS. However, compounds related

to P (e.g. $Mg(PO_3)_2$, $Mg_3(PO_4)_2$) were not confirmed by XRD, which indicates that they exist in non-crystal phase in the MAO coatings. As K_2ZrF_6 was added to the solution, diffraction peaks related to $Mg_2Zr_5O_{12}$ appeared. In the XRD pattern, the relative content of a certain phase increased, and the intensity of the diffracted rays increased [51]. As K_2ZrF_6 content increased in the solution, the relative strength of the $Mg_2Zr_5O_{12}$ (003) crystal face (2θ =30.644°, PDF 41-0185) increased, indicating that the $Mg_2Zr_5O_{12}$ relative content in the coating increased. Moreover, the relative strength of the main strong peak of the MgO (111) (2θ =43.037°, PDF 87-0653) reduced, indicating that its relative content in the coatings decreased. $Mg_2Zr_5O_{12}$ is a compound formed via solid solution reaction by MgO and ZrO_2 within a high temperature range of 2123–2373 K [52]. The production of $Mg_2Zr_5O_{12}$ could gradually reduce the content of elemental MgO, which was also benefit to improve the chemical durability of the MAO coating in moist or acidic environments.
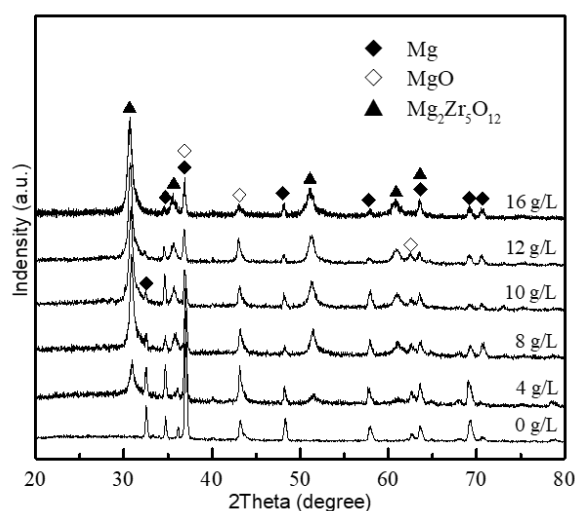

Figure 3. XRD patterns of the MAO coatings prepared in the base solution with various content of K_2ZrF_6, (a) 0 g/l, (b) 4 g/l, (c) 8 g/l, (d) 10 g/l, (e) 12 g/l, (f) 16 g/l.

The TEM micrographs of the MAO coating fabricated in the solution with 10 g/L K_2ZrF_6 are presented in Fig. 4. It is evident from Fig. 4(a) that the grain size of black particle is about 5-20 nm. HRTEM image of circled area in Fig. 4(b) displays two types of plane which correspond to (0 0 3) crystallographic plane of $Mg_2Zr_5O_{12}$ (d spacing 2.915 Å, PDF 41-0185) and (1 1 1) crystallographic plane of MgO (d-spacing 2.431Å, PDF 87-0653), respectively. Non-crystal phase also can be observed in the image. $ZrO_2 \cdot nH_2O$ colloidal particles in this solution system were nanoscale, and the size of ZrO_2 particles formed after drying and dehydration was considerably smaller than that of colloidal particles because of the double electric structure of colloidal particles. $ZrO_2 \cdot nH_2O$ particles entered into the spark discharge channels, dehydrated at high temperatures, and then converted to ZrO_2. MgO reacted with ZrO_2 to form a nanoscale $Mg_2Zr_5O_{12}$, and deposited onto the anode surface to form MAO coatings.
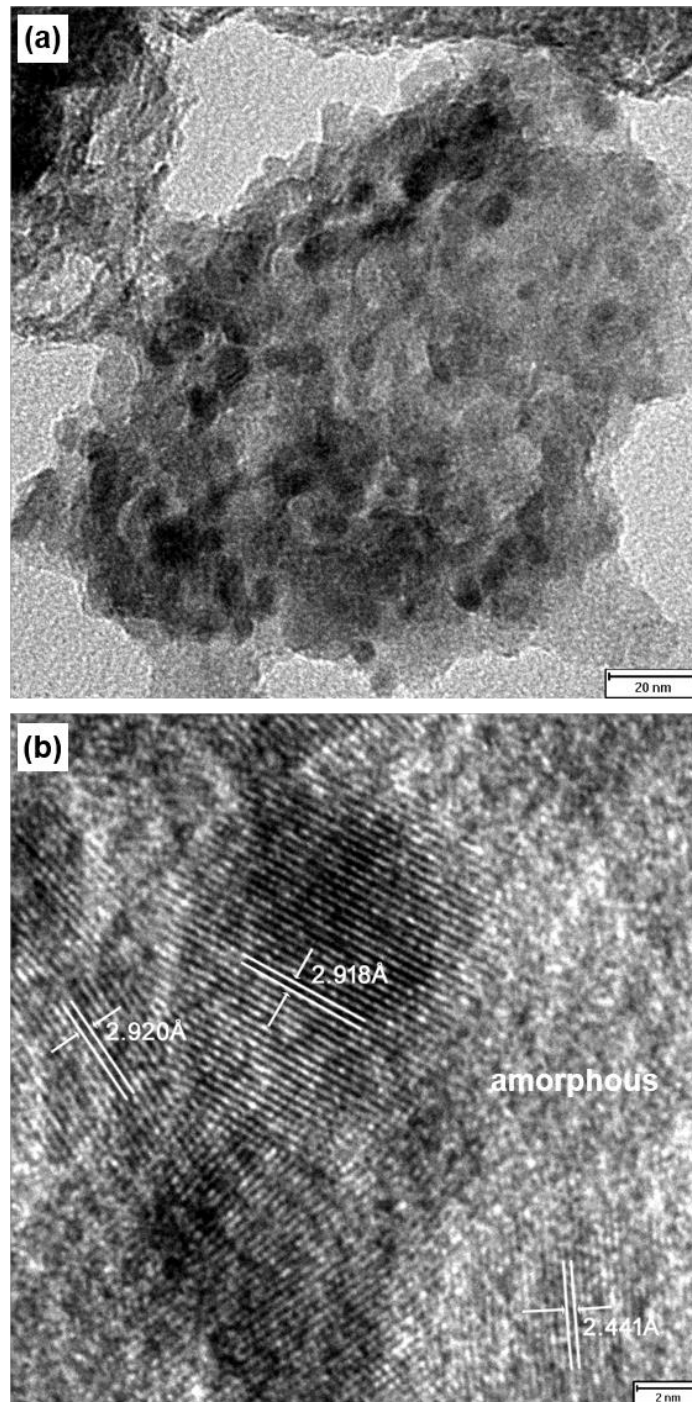
Figure 4. TEM (a) and HRTEM (b) image of the MAO coatings fabricated in the solution with 10 g/L K_2ZrF_6.

Fig. 5 shows the representative EIS testing results of the MAO coatings prepared in the solution with various content of K_2ZrF_6. Due to different morphology and phase structure, the MAO coating prepared in different solution displayed different corrosion behaviors in the EIS test. The EIS data can be analyzed with a circuit model, as shown in Fig. 6 [53–55]. As reported in previous studies, anti-corrosion property of the MAO coating depended largely on the inner compact layer (R_b), because this layer had more compact structure than the outer porous layer [56]. The average R_b value of different

MAO coatings are presented in Fig. 7. It was clear that added K_2ZrF_6 obviously improved the anti-corrosion property of the coating. With increasing K_2ZrF_6 content in the range from 0 – 10 g/L, the anti-corrosion property of the MAO coatings increased. However, anti-corrosion property of the coating gradually decreased when the K_2ZrF_6 content exceeded 10 g/L. It was indicated that at 10 g/L of K_2ZrF_6, the MAO showed the best corrosion resistance. It is widely accepted that anti-corrosion property of the MAO coating was influenced by its thickness, composition, phase composition, compactness, and surface defects (holes and cracks). The coating thickness gradually increased as K_2ZrF_6 content in the solution increased, as shown in Fig. 1. In general, the greater is the coating thickness, the better protection of the substrate will be. Holes and cracks are the weak parts of coatings, and these parts are relatively less resistant to Cl^- ions. Studies had revealed that these parts will even accelerate pitting corrosion of the substrate. Therefore, fewer holes and cracks in MAO coating produce smaller diameters, thus better protective effect on the substrate is achieved. As illustrated in Fig. 2(d), quite a few holes in the MAO coating fabricated in the solution with 10 g/L K_2ZrF_6 were mostly enclosed by oxidation reaction products. The composition and each phase relative content of the MAO coating obtained in different solutions showed obvious differences, as shown in Fig. 3. An increase in K_2ZrF_6 content increased the relative content of $Mg_2Zr_5O_{12}$ in the coatings. This increasing in relative $Mg_2Zr_5O_{12}$ content was also the reason for the difference in anti-corrosion property of these MAO coatings. Under synergy effect among these factors, the MAO coatings obtained when $Mg_2Zr_5O_{12}$ content was 10 g/L in the solution showed the best anti-corrosion property. Moreover, this solution was stable and could still be normally used after being stored for more than one year, and the prepared MAO coatings were basically no different from the fresh solution.
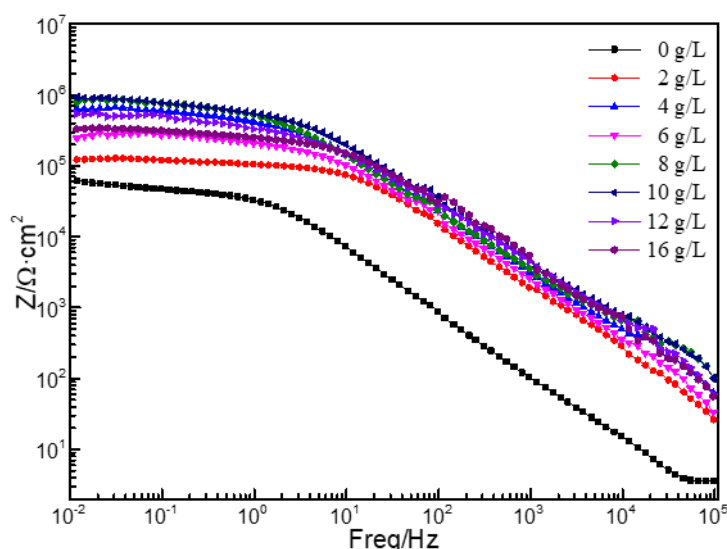

Figure 5. Bode plots of the MAO coatings prepared in the solution with various content of K_2ZrF_6.
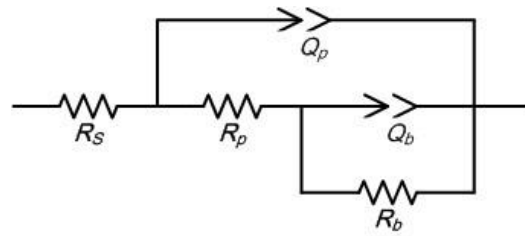
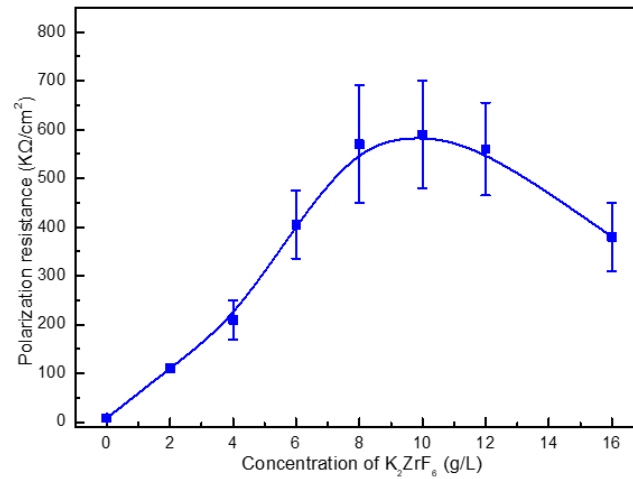**Figure 6.** Circuit model for fitting the EIS dates.

Figure 7. The R_b value of the MAO coatings fabricated in the solution with various content of K_2ZrF_6.

3.2 Effect of ZrO_2 nanoparticles

Many studies have demonstrated that nano- or micron-grade particles in Mg alloy MAO solution can participate in oxidation reactions, to change phase structures, to fill holes, and to improve anti-corrosion property [4,40,57]. Therefore, 2 g/L t-ZrO_2 nanoparticles were added to the solution consisted of K_2ZrF_6 (10 g/L), $(NaPO_3)_6$ (6 g/L), NaOH (3 g/L), and $(HOCH_2CH_2)_3N$ (10 ml/L) to study its influences on the characterization and anti-corrosion property of the MAO coating. ZrO_2 nanoparticles increased the thickness of the coating from 35 to 45 μm. Fig. 8 provides the surface morphology of the MAO coatings prepared in different solutions. For the coating prepared in the solution containing ZrO_2 nanoparticles, most holes were enclosed by sediments, and a large number of raised and small particles existed.
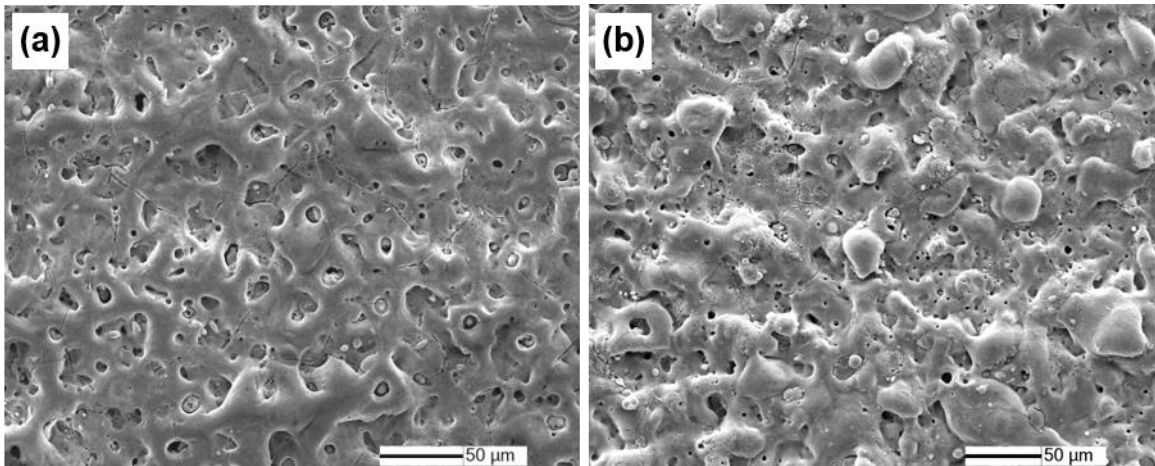
Figure 8. Surface morphology of the MAO coatings prepared in the solution containing 10 g/L K_2ZrF_6 without (a) and with (b) ZrO_2 nanoparticles.

Fig. 9 is cross section image (backscattered electron, BSE) of the MAO coatings. ZrO_2 nanoparticles improved the thickness and compactness of the MAO coating. In addition, high-brightness particles appeared in the coatings prepared in the solution with ZrO_2 nanoparticles. The BSE image can reflect the morphology and element distribution of the samples. Since the surface morphologies of the MAO samples can be ignored, Fig. 9 shows mainly the distribution of elements in the cross section image. The atom with a large atomic order produced more backscattered electrons, and the brightness in the graph was also high. The presence of highlighted particles in Fig. 9(b) also indicated that ZrO_2 nanoparticles were involved in oxidation films and played a role in filling the holes in the films and increasing their denseness.
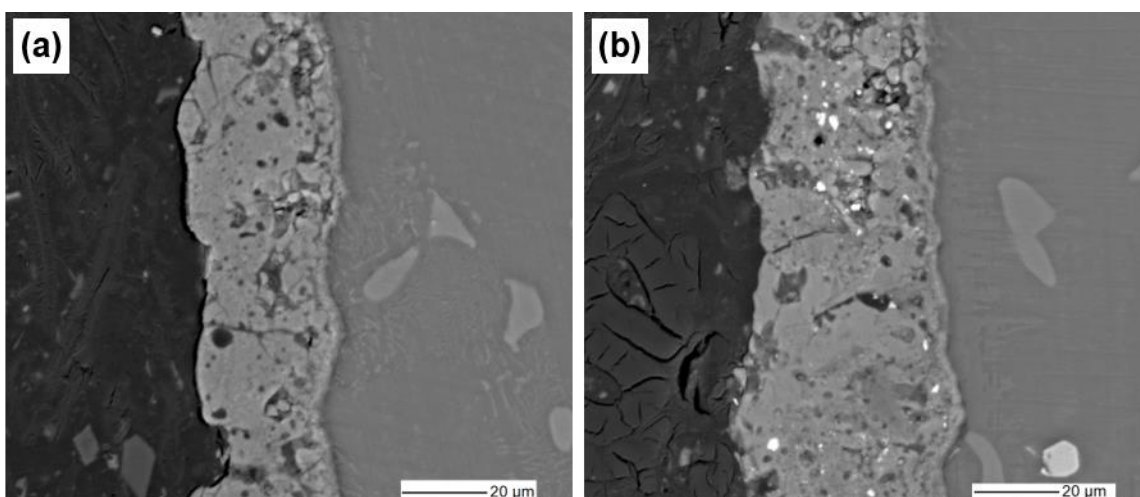

Figure 9. Cross section image (BSE) of the MAO coatings prepared in the solution containing 10 g/L K_2TiF_6 without (a) and with (b) ZrO_2 nanoparticles.

Fig. 10(a) displays the XRD patterns of the MAO coatings. The relative intensity of the main

peak of the coating obtained in the solution with ZrO_2 nanoparticles enhanced, which revealed that $Mg_2Zr_5O_{12}$ relative contents in this coating was higher than that formed in the solution without ZrO_2 nanoparticles. To further studied the influences of ZrO_2 nanoparticles on the phases of the coating, the XRD patterns from 29° to 33° are abstracted for further analysis, as displayed in Fig. 10(b). Observable peak shift happened, which should be attributed to the appearance of ZrO_2 phase. The broad peak at 29°–32° was a superposition of the (011) peak of t-ZrO_2 (PDF 50-1089) and the (003) peak of $Mg_2Zr_5O_{12}$ (PDF 41-0185).

Table 2. Fitting results of EIS data of the MAO coatings prepared in the solution containing 10 g/L K_2ZrF_6 with and without ZrO_2 nanoparticles.

Solution	R_s ($\Omega \cdot cm^2$)	R_p ($K\Omega \cdot cm^{-2}$)	n_p	Q_p ($S^{-1} \cdot s^n \cdot cm^{-2}$)	R_b ($K\Omega \cdot cm^2$)	n_b	Q_b ($S^{-1} \cdot s^n \cdot cm^2$)
Without ZrO_2	12.86	11.3	0.97	1.1×10^{-7}	550	0.55	8.89×10^{-7}
With ZrO_2	7.24	62.7	0.81	2.29×10^{-7}	890	0.62	4.0×10^{-7}

Fig. 11 shows the bode plots of the MAO coatings prepared in the solution containing 10 g/L K_2ZrF_6 with and without ZrO_2 nanoparticles. It can be seen that the two MAO coatings exhibit similar corrosion behavior, which indicating that their structure perpendicular to the direction of the substrate did not change. The EIS curves of the two MAO coatings were fitted with the equivalent circuit (as shown in Fig. 6), and the results are given in Table 2. For the coating prepared in the solution with ZrO_2 nanoparticles, it has higher resistance (R_p and R_b) than which formed in the ZrO_2 nanoparticles free solution, especially R_b was increased significantly from about 550 $k\Omega \cdot cm^2$ to 890 $k\Omega \cdot cm^2$. Added ZrO_2 nanoparticles enhanced the thickness and compactness of the MAO coating. Moreover, the size of the holes was reduced because of ZrO_2 nanoparticles, thereby reducing the corrosion of the MAO coatings by Cl^- ions.
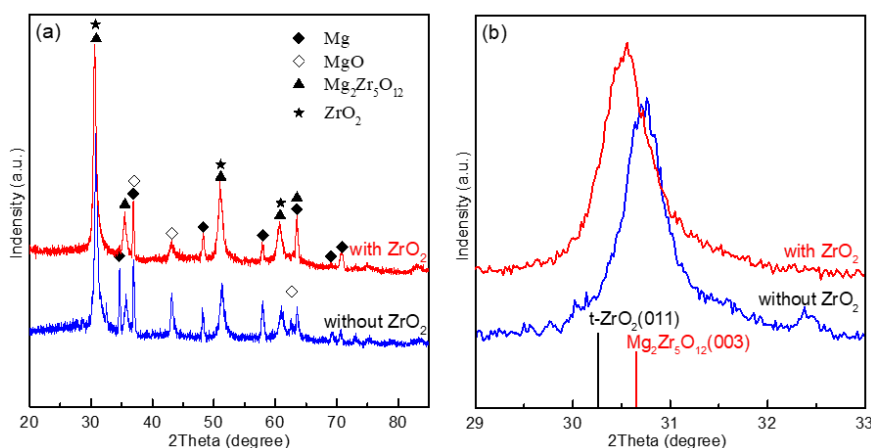

Figure 10. (a) XRD patterns of the MAO coatings prepared in the solution containing 10 g/L K_2TiF_6 with and without ZrO_2 particles, (b) XRD patterns between 29° and 33°.
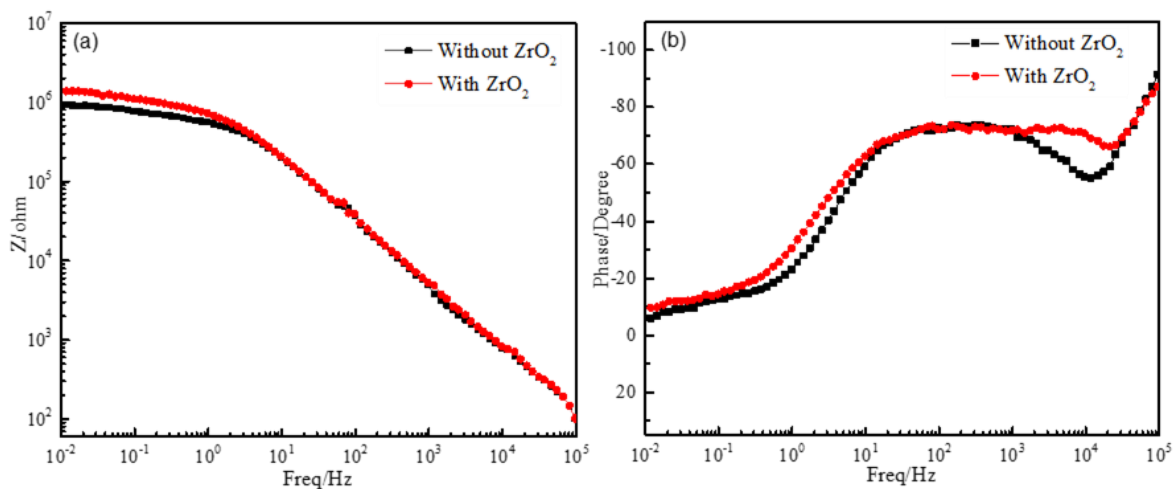
Figure 11. Bode plots of the MAO coatings prepared in the solution containing 10 g/L K_2ZrF_6.

4. CONCLUSIONS

1. Added K_2ZrF_6 in an alkaline phosphate solution increased the thickness of the MAO coating on AZ91D Mg alloy. Owing to self-sealing effect of the $ZrO_2 \cdot nH_2O$ colloidal particles originated from K_2ZrF_6, the size and quantity of holes in the MAO coatings decreased.

2. The MAO coating obtained in the K_2ZrF_6 free solution composed mainly of MgO and some non-crystal phosphate, and added K_2ZrF_6 induced nano Mg_2ZrO_{12} and reduced the relative content MgO in the MAO coating. The MAO coating fabricated in the solution with 10 g/L K_2ZrF_6 demonstrated the best compactness and anti-corrosion property.

3. t-ZrO_2 was detected in the MAO coating obtained in the solution with K_2ZrF_6 and t-ZrO_2 nanoparticles. Moreover, the thickness, compactness, and demonstrated of the MAO coating were further enhanced because of adding ZrO_2 nanoparticles.

References

1. A. Yerokhin, X. Nie, A. Leyland, A. Matthews, S. Dowey, *Surf. Coat. Technol.*, 122 (1999) 73.
2. G. Darband, M. Aliofkhazraei, P. Hamghalam, N. Valizade, *J. Magnes. Alloy,* 5 (2017) 74.
3. W. Zhang, B. Tian, Du, K. Du, H. Zhang, F. Wang, *Int. J. Electrochem. Sci.,* 6 (2011) 5228.
4. X. Lu, M. Mohedano, C. Blawert, E. Matykina, R. Arrabal, K. U. Kainer, M. L. Zheludkevich, *Surf. Coat. Technol.,* 307 (2016) 1165.
5. T.S.N.S. Narayanan, I. Park, M. Lee, *Prog. Mater. Sci.,* 60 (2014) 1.

6. Y. Gao, A. Yerokhin, A. Matthews, *Surf. Coat. Technol.,* 269(2015)170.
7. C. Liu, T. Xu, Q. Shao, S. Huang, B. Jiang, J. Liang, H. Li, *J. Alloys Comp.*, 784(2019) 414.
8. J. Liang, P. Bala Srinivasan, C. Blawert, W.Dietzel, *Corros. Sci.*, 51 (2009) 2483.
9. Y. Cui, Z. Hu, Y. Ma, Y. Yang, C. Zhao, Y. Ran, P. Gao, L. Wang, Y. Dong, D. Yan, *Surf. Coat. Technol.,* 363 (2019) 112.
10. J. Yu, G. Ji, Q. Liu, J. Zhang, Z. Shi, *Surf. Coat. Technol.,* 331(2017)21.
11. W. Mu, Y. Han, *Surf. Coat. Technol.,* 202(2008)4278.
12. Z. Yao, H. Gao, Z. Jiang, F. Wang, *J. Am. Chem. Soc.,* 91(2008)555.
13. L. Wang, L. Chen, Z. Yan, H. Wang, J. Peng, *J. Alloys Comp.,* 493 (2010) 445.
14. P. Bala Srinivasan, J. Liang, C. Blawert, W. Dietzel, *Appl. Surf. Sci.,* 256 (2010) 3265.
15. Y. Han, J.F. Song, *J. Am. Ceram. Soc.,* 92 (2009)1813.
16. J. Liang, P. Bala Srinivasan, C. Blawert, W. Dietzel, *Corros. Sci.,* 52 (2010) 540.
17. F. Liu, D. Shan, Y. Song, E. Han, *Surf. Coat. Technol.,* 206(2011) 455.
18. Y. Shi, J. Li, H. Wang，H. Teng, *Int. J. Electrochem. Sci.*, 15 (2020) 5846.
19. K. Lee, Y. Kim, H. Yang, J. Park, Y. Ko, D. Shin, *Mater. Charact.,* 99 (2015) 101.
20. Y. Zhu, W. Chang, S. Zhang, Y. Song, H. Huang, R. Zhao, G. Li, R. Zhang, Y. Zhang, *Coatings,* 9(2019) 197.
21. F. Einkhah, K.M. Lee, M.A.F. Sani, B. Yoo, D.H. Shin, *Surf. Coat. Technol.,* 238 (2014) 75.
22. K. Lee, Y. Ko, D. Shin, *J. Alloys Comp.,* 615 (2014) S418.
23. Z. Rehman, S. HunShin, I. Hussain, B. Koo, *Surf. Coat. Technol.,* 307(2016) 484.
24. H. Luo, Q. Cai, B. Wei, B. Yu, J. He, *J. Alloys Compd.*, 474 (2009) 551.
25. H. Luo, Q. Cai, J. He, B. Wei, *Curr. Appl. Phys.,* 9 (2009)1341.
26. Q. Cai, F. Liu, Q. Yan, Q. Luo, *J. Huazhong Univ. of Sci.& Tech.,* 39(2011)27. (In Chinese)
27. X. Cui, C. Liu, R. Yang, M. Li, X. Lin, *Surf. Coat. Technol.,* 269 (2015) 228.
28. L. An, Y. Ma, Y. Liu, L. Sun, S. Wang, Z. Wang, *Surf. Coat. Technol.,* 354 (2018) 226.
29. Z. Yao, Y. Xu, Y. Liu, D. Wang, Z. Jiang, F. Wang, *J. Alloys Comp.,* 509(2011)8469.
30. W. Mu, Y. Han, *Rare Metal Mat. Eng.,* 39(2010)1129.
31. J. Zhuang, Y. Guo, N. Xiang, Y. Xiong, Q. Hua, R. Song, *Appl. Surf. Sci.,* 357 (2015) 1463.
32. Z. Rehman, S. Shin, I. Hussain，B. Koo, *Prot. Met. Phys. Chem+,* 53 (2017) 495.
33. F. Liu, D. Shan, Y. Song, E.H. Han, *Trans. Nonferrous Met. Soc. China*, 21 (2011) 943.
34. F. Liu, D. Shan, Y. Song, E. Han, W. Ke, *Corros. Sci.,* 53(2011) 3845.
35. R. Arrabal，E. Matykina，F. Viejo，P. Skeldon，G. E. Thompson，M. C. Merino，*Appl. Surf. Sci.,* 254(2008) 6937.
36. R. Arrabal, E. Matykina, P. Skeldon, G. E. Thompson, *J. Mater. Sci.,* 43(2008) 1532.
37. A. Mandelli, M. Bestetti, A. Da Forno, N. Lecis, S. Trasatti, M. Trueba, *Surf. Coat. Technol.,* 205 (2011) 4459.
38. K. Lee，B. Lee，S. Yoon，E. Lee，B. Yoo，D. Shin, *Electrochim. Acta,* 67(2012)6.
39. T.S.N.S. Narayanan, M. Lee，*J. Colloid Interface Sci.,* 464 (2016) 36.
40. M. Asgari, M. Aliofkhazraei, Gh. Barati Darband, A. Sabour Rouhaghdam, *Surf. Coat. Technol.,* 383 (2020) 125252.
41. Z. Rehman, D. Choi*, J. Magnes. Alloy,* 7 (2019) 555.
42. Z. Rehman, S. Shin, H. Lim, B. Koo, *Surf. Coat. Technol.,* 311 (2017) 383.
43. K. Lee, K. Shin, S. Namgung, B. Yoo, D. Shin，*Surf. Coat. Technol.,* 205 (2011) 3779.
44. B. Jiang, D. Liu, *Chin. J. Nonferrous Met.,* 21(2011) 2402.
45. M. Tang, G. Li, W. Li, H. Liu, L. Zhu, *J. Alloys Comp.,* 562 (2013) 84.
46. M. Tang, W. Li, H. Liu, L. Zhu, *Curr. Appl. Phys.,* 12 (2012) 1259.
47. M. Tang, W. Li, H. Liu, L. Zhu, *Appl. Surf. Sci.,* 258 (2012) 5869.
48. M. Tang, Z. Feng, G. Li, Z. Zhang, R. Zhang, *Surf. Coat. Technol.,* 264 (2015) 105.
49. M. Tang, Z. Feng, X. Wu, W. Wang, G. Li, Z. Yan, R. Zhang, *Surf. Eng., In press*. DOI: 10.1080/02670844.2019.1635803

50. H. Duan, K. Du, C. Yan, F. Wang, *Electrochim. Acta,* 51 (2006)2898.
51. W. Xue, Z. Deng, Y. Lai, R. Chen, *J. Am. Ceram. Soc.,* 81 (1998) 1365.
52. M. Ray, D.R. Sahu, S.K. Singh, S. Verma, B.K. Roul, *Mater. Chem. Phys.,* 107(2008) 435.
53. M. Laleh, A. Sabour Rouhaghdam, T. Shahrabi, A. Shanghi, *J. Alloys Comp.,* 496(2010)548.
54. H. Duan, C. Yan, F. Wang, *Electrochim. Acta,* 52(2007)3785.
55. P. Bala Srinivasan, J. Liang, C. Blawert, M. Störmer, W. Dietzel, *Appl Surf Sci.,* 255 (2009) 4212.
56. S. Xia, R. Yue, R. Rateick, Jr., V. Birss, *J. Electrochem. Soc.,* 151(2004) B179.
57. B. Han, Y. Yang, H. Deng, Y. Chen, C. Yang, *Int. J. Electrochem. Sci.,* 13 (2018) 5681.